

# Shape Estimation of Space Debris Using Single-Range Doppler Interferometry

Toru Sato, *Member, IEEE*

**Abstract**—Shape estimation of space debris, or the fragments of satellites and rocket bodies left on the earth's orbit is an important task in evaluating its danger of a possible collision with operational spacecraft. A method of imaging a space debris whose size is smaller than the range resolution of the radar is proposed. It is called Single Range Doppler Interferometry (SRDI) in contrast to the conventional Doppler interferometry which reconstructs the two-dimensional image based on the high range resolution as well as the Doppler resolution. The proposed method makes use of the fact that space debris usually follow a simple spin motion around their major axis. Two-dimensional image of a target can be obtained by migrating the Doppler spectrogram over one spin period. The characteristics of the proposed SRDI method are examined by means of numerical simulation. For targets which consists of isolated isotropic scattering centers, clear image can be reconstructed with a resolution of half the radar wavelength, which is equivalent to the conventional RDI (or ISAR) technique that is applicable only when the range resolution of the radar is much finer than the size of the target. The image obtained from a conductive body is dominated by strong scattering centers which corresponding major reflections, although the size of the body could be roughly estimated.

**Keywords**—Radar imaging, remote sensing, shape estimation, space debris.

## I. INTRODUCTION

Space debris, or fragments of satellites and rocket bodies left on the earth's orbit, is now recognized as a serious environmental problem in the space [1], [2]. Since these objects have a very high velocity of more than 8 km/sec, which is one order higher than a ball, collision of a tiny debris with a spacecraft may cause a disaster. Monitoring is the first step to this environmental problem as is so for other problems.

Among various means of observing space debris, ground-based radar is the most powerful tool in observing objects on low-earth orbits. Shape estimation is an important issue in the observation of space debris, since it is directly related to the impact of collision. Statistical study has shown that their size estimated from the radar cross section (RCS) assuming a spherical shape do not agree with the size estimated from the atmospheric drag[3]. Analysis of RCS variations associated with the spin motion of space debris observed by a VHF radar suggests prolate shapes rather than spherical ones[4].

A commonly used technique for imaging a rotating object with a radar is the Range-Doppler Interferometry (RDI)[5], or the Inverse Synthetic Aperture Radar (ISAR) technique, in a different notation. This technique makes use of Doppler spreading of rotating target together with the conventional range gating in obtaining two-dimensional images of the target. It was first developed in the field of planetary radar astronomy[6], and has been utilized more recently in military imaging radars[7]. The application of this technique, however, has been limited to cases where the size of the target is much larger than the radar wavelength.

Toru Sato is with the Department of Electronics and Communication Engineering, Kyoto University, Kyoto 606-8501, Japan (e-mail: tsato@kuee.kyoto-u.ac.jp).

The most important target of future observations of space debris is those in the size region of 1–10 cm, because it is possible to protect spacecraft against small debris of less than 1cm by an appropriately designed shield, and those larger than 10cm has been constantly monitored by the existing network of radar and optical sensors around the world by the US SPACECOM[8].

In choosing the operational frequency of a debris radar, a higher frequency is better from the standpoint of sensitivity. On the other hand, a lower frequency provides a broader beamwidth and thus a higher detection rate of debris. The available transmitter power is also a decreasing function of the frequency. The compromise of the choice of frequency for a future debris radar will be in S- to X-band (10–3 cm wavelength). Obviously the conventional RDI technique cannot be applied to the imaging of small debris of 1–10 cm size at these frequency bands. Here we propose a technique which is applicable to the imaging of objects whose size is comparable to the radar wavelength.

## II. RDI AND SRDI

RDI makes use of the fact that echoes from different parts of a rotating object have different Doppler shifts. It has already been applied to the imaging of orbital objects, such as the case of Salyut-7/Kosmos-1686 complex body observed by X-band FGAN radar[9]. The size of the object in this case was about 200 wavelengths.

While the cross-range resolution is obtained by the Doppler effect, the range resolution is determined by the system bandwidth. Since the signal-to-noise ratio is inversely proportional to the bandwidth, its choice depends on the sensitivity of the system to the desired target. The very large scattering cross section of the satellite enabled the use of a wide bandwidth, and thus a finer resolution than the size of the target was obtained in the above case. Since the detection of objects in the size region of 1–10 cm at a distance of 100–1,000 km is a difficult task even with powerful radars, it is necessary to limit the system bandwidth narrow enough in order to assure the sensitivity to such small targets. It is not realistic to obtain a range resolution of less than 10 cm for such situation.

However, it is still possible to obtain a two-dimensional image using only the cross-range information if the same target can be observed for more than one spin period. We hereafter refer this method as Single Range Doppler Interferometry (SRDI) in contrast to RDI. Figure 1 schematically compares the two methods. With SRDI method, only the cross-range resolution is obtained at any instant, but the two-dimensional image can be retrieved by synthesizing the image over one spin period.

Here we assume that

1. the target is rotating at a constant angular velocity around its major axis, and

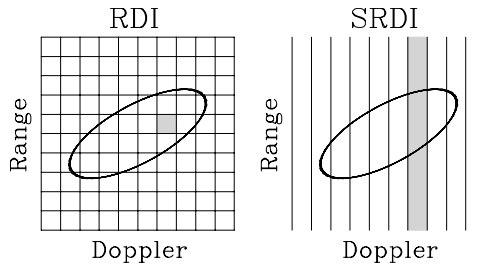


Fig. 1. DRI(ISAR) method and SRDI method.

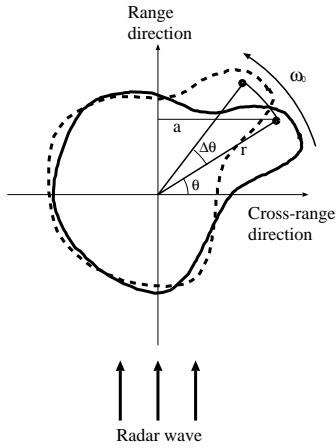


Fig. 2. Orientation of a rotating target.

2. the radar can observe the target for a period longer than its spin period.

The former assumption safely holds as far as the target has some internal loss, or dumping[10]. The latter assumption sets an important condition in designing the radar. The duration of observation, which is limited by the traverse time for a debris across the radar beamwidth, is usually a fraction of a second for a high-sensitivity radar if the beam direction is fixed, while the spin period may extend to a second or more even for the small objects of the current interest. Since the tracking of objects using a mechanically steered antenna is possible only for a target whose orbit is precisely known, it is essential that the radar has an electronic steerability of the antenna beam in order to monitor small objects which have not been cataloged.

The capability of active phased array radar for the monitoring of space debris has been demonstrated at VHF band[4], and unknown targets were tracked for about 10 sec, although the sensitivity was limited to the targets larger than 10 cm. Here we assume that the radar has such electronic steerability, and that the received echo is coherently detected at a sufficiently high sampling rate to detect the electric field variation associated with the spin motion of the target. We also assume that the mean Doppler shift due to parallel motion of the target is properly compensated for. If the radar system has a polarimetric capability, it would also provide the information of the target shape.

Let us consider a body rotating at the angular frequency  $\omega_0$  about its axis as shown in Fig. 2. The relative velocity of a point

$(r, \theta)$  in the body to the radar is given by

$$v_d = -\omega_0 r \cos \theta \quad (1)$$

Doppler shift of the radar echo from the point is thus given as

$$\begin{aligned} \omega_d &= \frac{4\pi}{\lambda} v_d \\ &= -\frac{4\pi\omega_0}{\lambda} r \cos \theta \\ &= -\frac{4\pi\omega_0}{\lambda} a, \end{aligned} \quad (2)$$

where  $\lambda$  is the radar wavelength, and  $a$  is the cross-range distance. The cross-range resolution is thus related to the Doppler frequency resolution  $\Delta\omega_d$  as

$$\Delta\omega_d = \frac{4\pi\omega_0}{\lambda} \Delta a. \quad (3)$$

The Doppler frequency resolution is limited by the duration of observation  $T$ , and thus by the range of rotational angle  $\Delta\theta$  used in the imaging of each part of the target as

$$\Delta\omega_d \simeq \frac{2\pi}{T} = \frac{2\pi\omega_0}{\Delta\theta}. \quad (4)$$

As a result, the cross-range resolution of RDI is given by

$$\Delta a \simeq \frac{\lambda}{2\Delta\theta}. \quad (5)$$

The cross-range resolution of SRDI is of course equivalent to that of RDI. While  $\Delta a$  becomes smaller by choosing larger  $\Delta\theta$ , the image smears out because different parts of the target are used in the imaging of a point. Here we set the upper limit of  $\Delta\theta$  to about 1 radian aiming to image the rough shape of the entire body.

It should be noted that  $\Delta\theta$  itself cannot be directly measured, which means that we cannot distinguish a small body with a large angular velocity from a large body spinning slowly. In our case, however, the rotation period can be determined by tracking the target for more than one spin period, and by taking auto-correlation of the received signal.

### III. SIGNAL PROCESSING OF SRDI

In SRDI, we need to represent the Doppler spectrum of the target as a function of rotation angle  $\theta$ . The Doppler shift of the radar echo from a point whose original position is  $(r, \theta_0)$  is given by

$$\omega_d(\theta) = -\frac{4\pi\omega_0}{\lambda} r \cos(\theta + \theta_0). \quad (6)$$

Figure 3 shows an example of the received signal time series for a point target located at  $(2\lambda, 0^\circ)$ . The solid and dashed curves show the output of the in-phase and quadrature channels of a coherent receiver, respectively. The ordinate is normalized to an arbitrary scale. While the periodicity of the signal varies as the angle changes, the two curves keeps constant phase difference of about  $90^\circ$ . The highest instantaneous frequency seen at  $0^\circ$ ,  $180^\circ$ , and  $360^\circ$  corresponds to the fastest motion of the target relative to the radar when the target is located in the cross-range direction

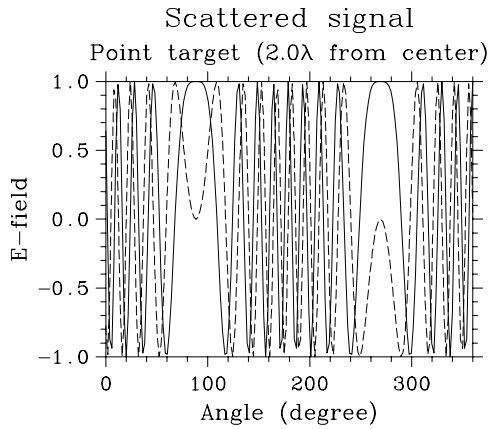


Fig. 3. Normalized scattered signal of a point target located at  $2\lambda$  from the center versus the rotation angle.

in Fig. 2, and the stationary phase found at  $90^\circ$  and  $270^\circ$  indicates the zero-Doppler condition met when the target is in the range direction. It is thus possible to directly relate the instantaneous frequency of the signal to the relative location of the target to the center of rotation.

In an actual observation, the abscissa is expressed in terms of time  $t$  instead of angle  $\theta$ . We first need to take the auto-correlation function of the received time series to find the periodicity due to spin motion. After determining the spin frequency  $\omega_0$  from this analysis, we can convert  $t$  into  $\theta$  as shown in Fig. 3. The Doppler frequency is further converted to apparent radius by

$$r(\theta) = \frac{\lambda}{4\pi\omega_0} \omega_d(\theta) \quad (7)$$

While the instantaneous frequency can be easily determined for such a simple case by taking the derivative of the phase versus  $\theta$ , it is not straight forward in the general case where the received signal contains echoes from various parts of the target. It is especially so for the case  $r \sim \lambda$ , where  $\omega_d(\theta)/\omega_0$  is only on the order of 10.

A number of time-frequency distribution techniques have been proposed for such a situation to obtain high frequency and time resolutions simultaneously [11]. However, here we use the simplest and most stable method of the short-time Fourier transform (STFT). The spectrogram, or the time-frequency power spectrum, is given by the STFT method as

$$S(t, \omega) = \left\{ \int s(t') w(t' - t) e^{-j\omega t'} dt' \right\}^2, \quad (8)$$

where  $s(t)$  is the signal, and  $w(t)$  is the window function. As easily understood from this equation, narrowing the window  $w(t)$  in order to achieve a better time resolution causes smearing of the spectrum in the frequency domain, because the Fourier transform of  $w(t)$  broadens. The spectrogram reduces to the conventional power spectrum when  $w(t) = 1$ , and to  $s(t)^2$  when  $w(t)$  is the delta function.

The image versus angle and the apparent radius is thus given by

$$S(r, \theta) = \left\{ \int_0^{2\pi} s(\theta') w(\theta' - \theta) e^{-j\omega_d \theta'} d\theta' \right\}^2 \quad (9)$$

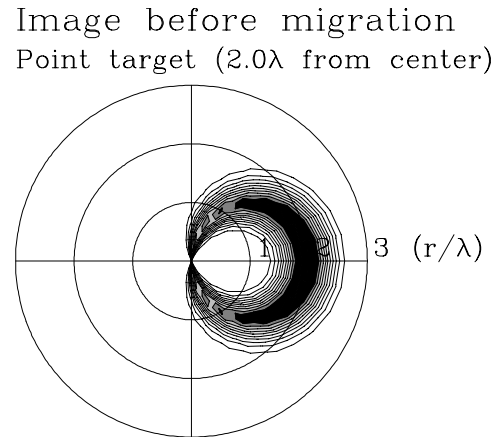


Fig. 4. Doppler spectrum of a point target located at  $2\lambda$  from the center versus the rotation angle.

where  $s(\theta)$  is the complex receiver output at angle  $\theta$ , and  $w(\theta)$  is a raised cosine window of the half angular width of  $30^\circ$  as given by

$$w(\theta) = \begin{cases} (1 + \cos 6\theta)/2 & (-\pi/6 < \theta < \pi/6) \\ 0 & (\theta < -\pi/6, \theta > \pi/6) \end{cases}$$

The radius  $r$  is related to  $\omega_d$  via Eq. 7.

Figure 4 shows this image on a polar coordinate as an isopower contour map. As expected from Eq. 6, the signal from a point target makes a circular trace on this figure. It is found that the SRDI imaging is a process to convert a delta function located at  $(2\lambda, 0^\circ)$  into the distributed image as shown in this figure, which can be interpreted as the two-dimensional impulse response, or the smoothing function. Since this distribution is known, the image interpretation of SRDI is regarded as the inverse problem to eliminate the effect of this smoothing function.

The simplest method for this is the deconvolution. It is to take the two-dimensional Fourier transform of the given image, divide it by the Fourier transform of the smoothing function, and then take the inverse Fourier transform. However, the deconvolution, or similar super-resolution techniques, are not applicable when the signal-to-noise ratio is low, because they tend to enhance fluctuations due to noise.

The opposite approach is to apply the matched filter. It is to apply the same smoothing function once again to the obtained image. The idea is to enhance the area where the signal contribution is largest in the impulse response. This method is stable in the presence of strong noise, as is the case of our current concern, but is apparently poor in terms of the resolution.

Migration is a technique based on a similar idea as the matched filter, and is widely used in the field of geophysical prospecting [12]. It is often encountered in observations that a group of points in the observed image have equal probability as the candidate of the actual location of the target. In our case, all points on a circle of radius  $r$  centered at  $(r, \theta)$  are the candidates of the source that produced an image obtained at point  $(2r, \theta)$ . So we re-distribute the intensity of each measured point of the image

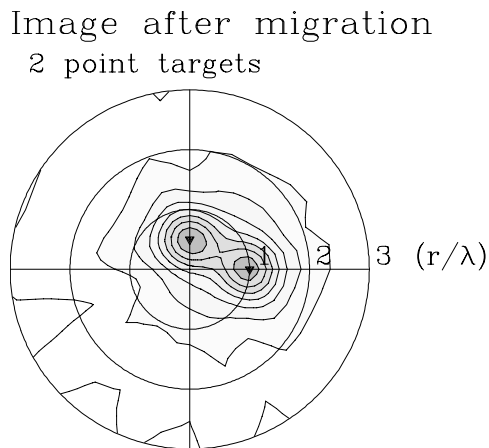


Fig. 5. Image of two point targets after the migration. Triangles denotes the location of given point targets. Contours are drawn at an equal interval of the intensity, and normalized to the peak value in the figure.

over this circle. This procedure is expressed as

$$S_m(r, \theta) = \frac{1}{2\pi} \int_0^{2\pi} S(r \cos\{\theta' - \theta\}, \theta') d\theta'. \quad (10)$$

It is readily understood that all these circles cross at the correct position of the target, which is high-lighted.

An example of this procedure for two point targets at radius  $2\lambda$  and  $1\lambda$ , respectively, is shown in Figure 5. The contours are drawn at an equal interval of the intensity, and normalized to the peak value in the figure. This figure demonstrates that SRDI method has a resolution (half-power width) of about  $1/2\lambda$ , which is the same as the cross-range resolution of RDI shown in Eq. 5.

#### IV. SCATTERING FROM A CONTINUOUS BODY

The above simulation assumed isotropic point targets, and more over, the linear superposition of multiple targets, which is equivalent to assume weak (or Born) scattering. The actual target usually consists of a continuous body, along which the induced current due to the incidental electric field flows. If the body consists of non-conductive material whose relative dielectric constant is close to one, the above model which assumed superposition of point scatterers would be still valid. However, the echo intensity will be very weak for such cases. If, on the other hand, the body is made with metallic material, the scattered field from the body will be dominated by the reflection and refraction.

In conventional RDI, which deals with a body whose dimension is much larger than the radar wavelength, the reconstructed image shows the location of strong scattering centers such as the apexes and edges which usually represents the outer shape of the body. The relation of the physical shape of the target and the scattered field is readily obtained by numerical methods such as the geometrical theory of diffraction, which makes use of high-frequency approximations. Although the location of scattering centers moves as the target rotates, it does not largely affect the image since the image is obtained from the scattered field of a limited angular range of rotation. In our situation where the tar-

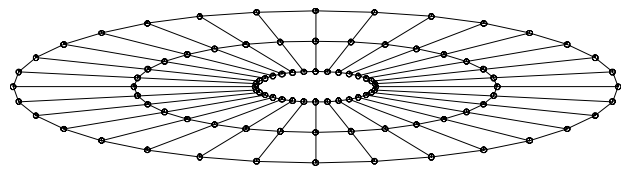


Fig. 6. Wire grid model of a  $4\lambda \times 0.5\lambda$  ellipsoid.

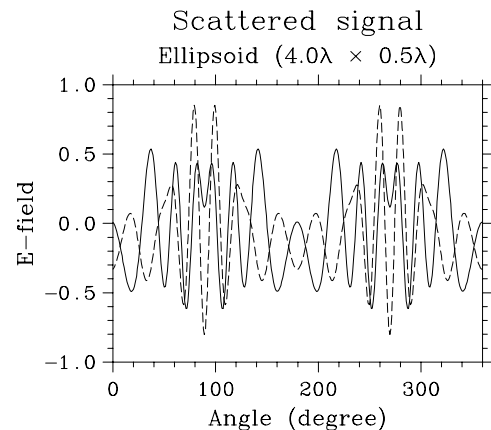


Fig. 7. Scattered signal (I and Q channel) from a conducting elliptic plate shown in Fig. 6.

get size is on the order of the radar wavelength, it is anticipated that the change of scattering centers due to the entire spin period is substantial, and thus may seriously distort the image.

In order to simulate the scattered field from a continuous conductive body, a two-dimensional wire grid approach is taken. For simplicity, elliptic plates of various size and shape are considered. Figure 6 shows the model of a  $4\lambda \times 0.5\lambda$  ellipsoid. The elliptic plate is divided into 32 and 2 sectors in the angular and radial directions, respectively, and the radius of each wire is set to  $0.005\lambda$ . Assuming a partial sinusoidal current distribution function on each element of the grid, the scattered field is computed by the moment method.

Figure 7 shows the scattered signal from the elliptic plate of Fig. 6 computed by this method. The enhanced echoes at around  $90^\circ$  and  $270^\circ$  indicate the dominant reflection which occurs when the major axis of the ellipse becomes perpendicular to the direction of the incident wave. The image generated from this data is dominated by these components, and only the two strong scattering centers are identified in the image. This is also the case for conventional RDI method, but it is not as serious as the present case because a large body may have a number of outstanding scattering centers which more or less represent the outline of the target. It should be noted here that the correct image of a perfectly conducting sphere cannot be obtained with RDI either, because the rotation does not affect the scattered field at all.

In order to reduce the prominence of these strong scattering centers, the power of the spectrogram at each  $\theta$  is normalized by the total reflection power at each angle before applying the

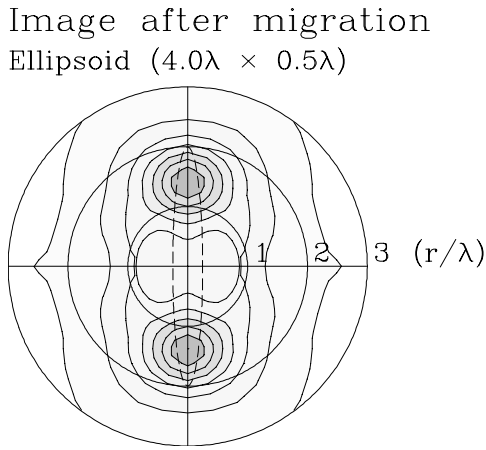


Fig. 8. SRDI image of a conducting elliptic plate shown in Fig. 6. Dashed curve shows the given shape.

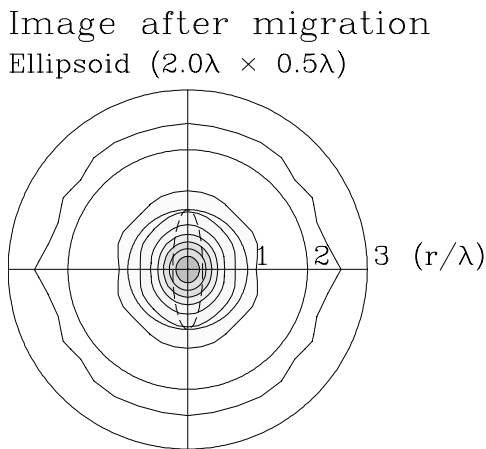


Fig. 9. Same as Fig. 8, but for an elliptic plate of  $2\lambda \times 0.5\lambda$ .

migration operation. The normalized spectrogram given by

$$S_n(r, \theta) = S(r, \theta) / \int_{-\infty}^{\infty} S(r, \theta') d\theta' \quad (11)$$

is substituted for  $S(r, \theta)$  on the right hand side of Eq. 10. Figure 8 shows the result of imaging of a perfectly conducting elliptic plate of  $4\lambda \times 0.5\lambda$ . Although the two prominent points are still emphasized in the reconstructed image, the prolate shape of the body and its size can be roughly estimated.

For smaller elliptic plates, the prominent points tend to collapse into single point, and thus it becomes harder to identify the entire shape of the target. Figure 9 shows the image for an elliptic plate of  $2\lambda \times 0.5\lambda$ .

### V. ANGULAR AMBIGUITY

We have so far assumed that the spin period of the target can be correctly estimated by examining the periodicity of the scattered signal. This assumption is valid when the target has an irregular shape with no inherent axis of symmetry, as is generally believed to be the case for small space debris.

However, the estimated period may be shorter than the true spin period if the shape of the target has symmetry axes, such

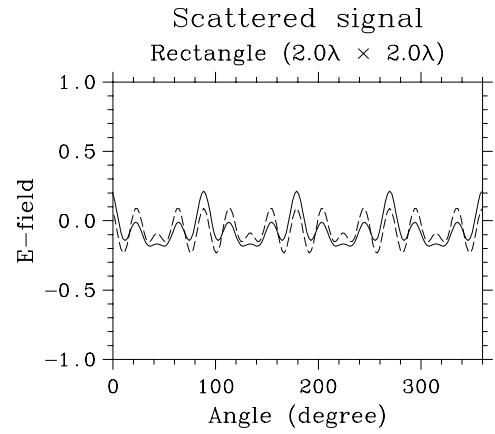


Fig. 10. Scattered signal from a conducting square plate.

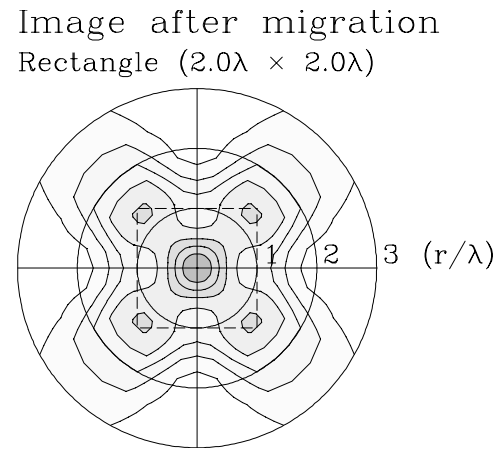


Fig. 11. SRDI image of a conducting square when the spin period is correctly estimated. Dashed curve shows the given shape.

as the case for a rocket body. For such cases, the estimated spin period estimated from the periodicity of the echo will be half of the real period, or even shorter if there are more than one axes of angular symmetry. The proposed method apparently does not work properly under these conditions. Here we briefly examine the possible effect of this ambiguity.

Figure 10 shows the scattered electric field computed for a conducting square plate. As shown in the figure, the scattered signal shows a periodicity of  $90^\circ$ . Although it is not likely that the real debris has such pure symmetry, the periodicity estimation based on the autocorrelation analysis of the received signal time series may result in the shorter estimate if the target has a quasi symmetry in its shape. Figure 11 is the SRDI image of this object when the spin period is correctly estimated. Four corners of the square is clearly marked as outstanding scattering centers in the image.

Figure 12 shows the same image when the spin period is incorrectly estimated to be the half of its true value. As easily imagined, the reconstructed image has two outstanding edges instead of the four in the correct image. It should be noted, however, that the size of the estimated image roughly agrees with the real size of the target. While the physical size of the target should be

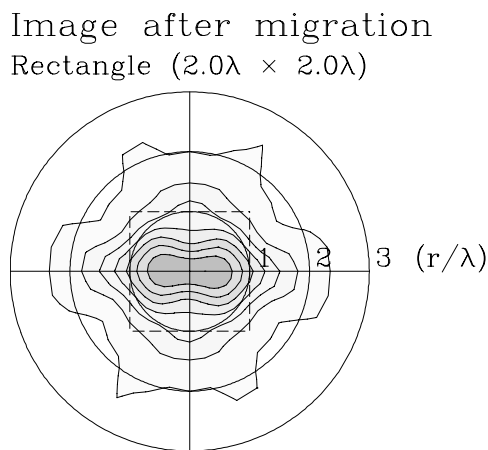


Fig. 12. SRDI image of a conducting square when the spin period is incorrectly estimated to be half of the true period.

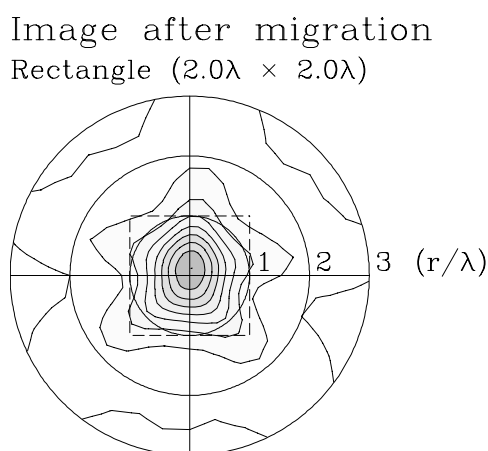


Fig. 13. SRDI image of a conducting square when the spin period is incorrectly estimated to be  $1/4$  of the true period.

estimated as half of the true size when the target is considered as having only two corners instead of the four, the radius of the corner from its center of the rotation is estimated to be twice the real value because the Doppler velocity is also over-estimated by a factor of two. As a result, the target is estimated to be an object of about the size of the real plate although the shape estimation is incorrect. Figure 13 shows the case when the spin period is estimated as  $1/4$  of the true period. In this case, only one strong scattering center is observed at the center of its rotation. The radial extent of the target again roughly covers its true aperture due to the same effect as is the case for Fig. 12.

In real observational situations of space debris, such symmetry usually occurs for known targets as working or abandoned satellites and rocket bodies, for which the shape information is available. Since our main interest is in determining the shape of unknown objects, it will be rather rare that the cases considered in this section become real problem.

## VI. SUMMARY

A method of imaging a space debris whose size is smaller than the range resolution of the radar is proposed. The proposed

method makes use of the fact that space debris usually follow a simple spin motion around their major axis. Two-dimensional image of a target can be obtained by migrating the Doppler spectrogram over one spin period.

The characteristics of the proposed SRDI method are examined by means of numerical simulation. For targets which consists of isolated isotropic scattering centers, clear image can be reconstructed with a resolution of half the radar wavelength, which is equivalent to the conventional RDI (or ISAR) technique that is applicable only when the range resolution of the radar is much finer than the size of the target.

The image obtained from a conductive body is dominated by strong scattering centers which corresponding major reflections, although the size of the body could be roughly estimated. If the estimated spin period is in error, which may occur in rather rare situations of unknown targets with symmetrical shapes, the rough size of the target is still correctly estimated although the shape can no more be reconstructed. Further study is needed to properly interpret the image of a continuous body.

## REFERENCES

- [1] National Research Council, *Orbital debris, A technical assessment*, 210 pp., National Academy Press, Washington, D.C., 1995.
- [2] N.L. Johnson and D.S. McKnight, *Artificial space debris*, 111 pp., Orbit Book Company, Florida, 1987.
- [3] G.D. Badhwar and P.D. Anz-Meador, "Determination of the area and mass distribution of orbital debris fragments," *Earth, Moon, and Planets*, vol. 45, no. 4, pp. 29–51, 1989.
- [4] T. Sato, T. Wakayama, T. Tanaka, K. Ikeda and I. Kimura, "Shape of space debris as estimated from RCS variations," *J. Spacecraft Rockets*, vol. 31, no. 4, pp. 665–670, 1994.
- [5] J. L. Walker, "Range-Doppler imaging of rotating objects," *IEEE Trans. Aero. Electr. Systems*, vol. AES-16, no. 1, pp. 23–52, 1980.
- [6] T. Hagfors and D.B. Campbell, "Mapping of planetary surface by radar," *Proc. IEEE*, vol. 61, no. 9, pp. 1219–1221, 1973.
- [7] D. L. Mensa, *High resolution radar cross-section imaging*, 270 pp., Artech House, Boston, 1991.
- [8] P. A. Jackson, "Space surveillance satellite catalog maintenance," *Orbital Debris Conference, AIAA-90-1339*, 1990.
- [9] D. Mehrholz, "Radar tracking and observation of noncooperative space objects by reentry of Salyut-7/Kosmos-1686," *Proc. Internat. Workshop on Salyut-7/Kosmos-1686 Reentry*, vol. ESA SP-345, pp. 1–8, 1991.
- [10] V. A. Chobotov, *Spacecraft attitude dynamics and control*, 140 pp., Krieger Publishing Co., Malabar, Florida, 1991.
- [11] D. L. Jones and T.W. Parks, "A resolution comparison of several time-frequency representations," *IEEE Trans. Sig. Proc.*, Vol.40, pp.413–420, 1992.
- [12] B. D. Milton and C. H. Savit, "Introduction to geophysical prospecting," Fourth Ed., 867 pp., McGraw-Hill, New York, 1988.

**Toru Sato** received his B.E., M.E., and Ph.D. degrees in electrical engineering from Kyoto University, Kyoto, Japan in 1976, 1978, and 1982, respectively. He has been with Kyoto University since 1983 and is currently a Professor of Department of Communications and Computer Engineering, Graduate School of Informatics. His major research interests have been system design and signal processing of atmospheric radars, radar remote sensing of the atmosphere, observations of precipitation using radar and satellite signals, radar observation of space debris, and signal processing for subsurface radars. He was awarded Tanakadate Prize in 1986. He is a member of the Institute of Electrical and Electronics Engineers, the Institute of Electronics, Information, and Communication Engineers of Japan, the Society of Geomagnetism and Earth, Planetary and Space Sciences, the Japan Society for Aeronautical and Space Sciences, and American Meteorological Society.